Supporting Information

Shi et al. 10.1073/pnas.1220794110

SI Text

The db^-/db^- mouse was originally discovered in an inbred strain of mouse, where diabetes is inherited as an autosmal recessive phenotype characterized by metabolic disturbances resembling diabetes mellitus in man: that is, hyperphagia, obesity, lipidemia, hyperinsulinemia, and insulin resistance (1). The *db* gene encodes a G-to-T point mutation of the leptin receptor, resulting in abnormal splicing and defective receptor for leptin (2, 3). It was more recently discovered that this mutation is related to the obese gene (4), the receptor for leptin (5).

The db^-/db^- mouse is just one of many rodent diabetes models. Other early models include alloxon diabetic rats (6, 7) and streptozotocin (STZ)-diabetic rats (8). Type 1 and type 2 models encompass both genetic and chemically induced approaches (9–12). Moreover, The Animal Model of Diabetic Complications Consortium at the National Institutes of Health aims at generating appropriate and relevant models (12). Further examples of type 2 diabetes models include the BBZDR-WOR rats (13), Zucker fatty rats (14), the Goto-Kakizaki (GK) rat (15), and the ob/ob mouse (16).

SI Discussion

Observational Errors in the Measurements. The results from the in vivo and in vitro measurements were compatible, although the significance levels differed, the in vivo results being more significant than the in vivo results. An analysis of the observational errors showed, however, that the error of the in vitro estimates was considerably less than the in vivo estimates; 1.3 m/s vs. 12.9 m/s. The calculation was based on the following error propagation equation (17):

$$\Delta v = \sqrt{\Delta s^2 \left(\frac{1}{t}\right)^2 + \Delta t^2 \left(\frac{s}{t^2}\right)^2},$$

where Δv, Δs, and Δt are the uncertainties in velocity, distance, and time, respectively. For the in vivo experiments, an upper bound for Δs was estimated to 1.0 mm and for Δt to 50 μs. The average time t was 0.19 ms and the average distance 8.5 mm. Hence, the observational error of Δv was less than 12.9 m/s. For the in vitro measurements, an upper bound for Δs was estimated to 0.5 mm and for Δt to 50 μs, and the average quantities were 0.57 ms and 6.0 mm, for the time and distance, respectively. Therefore, the observational error Δv for the in vitro experiments was less than 1.3 m/s.

Temperature Dependence. The conduction velocities (CVs) of the in vivo experiments were approximately fivefold higher than the in vitro ones. The temperatures were 34–36 °C and 22 °C, respectively. The termperature coefficient is typically around 3 (18-20).

Neuron Loss and Apoptosis. Evidence for neuronal apoptosis has been obtained in other experimental in vitro and in vivo models. High glucose concentrations (at least 45 mM) can induce apoptosis in embryonic dorsal root ganglion (DRG) neurons grown in culture by compromising mitochondrial function (21–24). In vivo evidence for apoptosis of DRG neurons has been demonstrated in the STZ rat model by some groups (23, 25) but not by others (26, 27). Wright et al. (28) found expression of activating transcription factor 3 (ATF3), a marker for lesioned neurons (29) in DRGs of STZ mice.

Neuron Loss and GalR2-KO Mice. Galanin is a neuropeptide (30) acting via three cloned receptors, GalR1 to -3 (31). We have previously studied a GalR2 KO mouse (32). The number of DRG neurons was low in the KO mouse, ∼20% less than in WT mouse, which is similar to the number seen in WT mouse 7 d after a peripheral axotomy (32, 33). Furthermore, axotomy did not cause any further loss of DRG neurons in the GalR2 KO mouse; that is the number of neurons was the same on the ipsi- as on the contralateral side (32), mimicking the situation in the db^-/db^- mouse. It is an intriguing question whether or not the 20% of DRG neurons lost after axotomy in WT mouse represent the same populations of DRG neurons lost in the db^-/db^- mouse (present results), as well as are absent in the GalR2-KO mouse.

Phenotypic Changes in Diabetic Peripheral Neuropathy. Except for the reduction in PLCβ3 levels in the db^-/db^- mouse, we did not observe any major changes in a number of other markers [e.g., calcitonin gene-related peptide (CGRP), substance P, galanin, superoxide dismutase 2 (SOD2), neuropeptide tyrosine (NPY) Y1 receptor, neuronal nitric oxide synthase (nNOS), ATF3, Iba1, p-p38, glial fibrillary acid protein (GFAP), NF200, IB4, or the P2 × 3 receptor]. Zochodne et al. (34), in an extensive analysis of rats after STZ treatment for 2 or 12 mo, found no changes at 2 mo, but down-regulation of mRNA levels of transcripts for pituitary adenylate cyclase-activating peptide (PACAP), substance P, NFM, p75, trkA, trkC and, especially, CGRP was observed at 12 mo. A down-regulation of CGRP (35, 36) and substance P (37–39) is also seen after peripheral nerve injury, suggesting that the down-regulations reported by Zochodne et al. (34) at 12 mo in the STZ rat can be because of injury to unmyelinated and thin myelinated axons. Interestingly, however, no up-regulation was observed for several neuropeptide transcripts [vasoactive intestinal polypeptide (VIP), galanin, cholecystokinin (CCK), PACAP] (34), known to be up-regulated after peripheral nerve injury (40–42), suggesting that diabetic peripheral neuropathy (DPN) is different from mechanical nerve injury.

Using both gene array and Western blotting, Burnand et al. (43) have analyzed DRGs of 8-wk-old rats with STZ-induced diabetes, and they reported that nerve injury-responsive genes coding for growth-associated protein 43, galanin, NPY, prepro-VIP, nNOS, protease nexin 1, heat-shock 27, and myosin light-chain kinase II were not changed compared with control animals, indicating that no nerve injury-induced phenotype is established. The authors further showed that many well-known proapoptotic genes were also unaltered in STZ rats, such as Bax, Bad, Bid, c-jun, p38, TNFR1, caspase 3, and NOS2. In addition, antiapoptotic genes, such as Bcl-2, Bcl-xl, Bcl-w, and NF-κB, were unchanged. Brussee et al. (44) demonstrated that, although a trend of up-regulation of mRNA levels was seen for heat shock protein, for the α2δ1 calcium channel subunit and phosphatidylinositol 3-kinase in DRGs in a long-term (4 mo) type 2 diabetes model in rat, the results were not statistically significant. Interestingly however, p-p38 is up-regulated in the DRGs of 8-wk-old db^-/db^- mice but dramatically reduced at 12 wk of age (WoA) (45).

Possible Role of Phospholipase C β3. Phospholipase C β3 (PLCβ3) is downstream of several G protein-coupled receptors, which are activated by, among others, neuropeptides, such as galanin and CCK, and other ligands (46). Receptors for galanin and CCK are expressed in subpopulations of rodent DRG neurons (47–50), whereby the CCKB receptor is dramatically up-regulated after axotomy (50), and activation of both GalR2 and CCKB receptor

presumably causes increase in intracellular Ca^{2+} via PLCβ3 and release of excitatory transmitters, such as glutamate: that is, the enzyme is pronociceptive.

Treatment with Antioxidants. A relationship between the pathogenesis of diabetes and coenzyme Q10 (CoQ10) deficiency has been identified by Quinzii and Hirano (51). Antioxidant processes may play an important role in protection against the onset and progression of DPN, such as promotion of neuronal survival, stimulation of nerve repair, and even induction of nerve regeneration under diabetic conditions (52–59). Free radicals and reactive oxygen species are eliminated by antioxidants, among which the lipid-soluble antioxidant CoQ10 is particularly powerful (60–65).

SI Materials and Methods

Animals. C57BL/KsJm/*Leptdb* (db^-/db^-) mice (Stock 000662) and their normoglycemic heterozygous littermate (as control) mice were obtained from Charles River Laboratories. The mice were housed five per cage in a 12-h light/dark cycle at 22 °C and provided ad libitum with standard laboratory food and water. CoQ10 was added to the food from the age of 7 wk to pellets at a concentration of 1 g/kg. The experimental procedures were approved by the North Stockholm Ethical Committee for Care and Use of Laboratory Animals. The design of the experiment is shown in Fig. S1.

Nerve Injury Model. Animals were anesthetized with isoflurane (1.7–2.0% vol/vol), and the left sciatic nerve was transected at midthigh level (around 20 mm distal to the DRG). A 5-mm portion of the nerve was resected, and the proximal end was ligated to prevent regeneration. The animals were allowed to survive for 7 d after surgery.

Behavioral Tests. Animals were placed in transparent plastic domes on a metal mesh floor with a hole-size 2 × 3 mm. After 30-min habituation, for the tactile allodynia test the threshold for hind paw withdrawal (both sides) was measured by graded-strength von Frey monofilaments (0.4, 0.6, 1.0, 1.4, 2.0, 4.0, and 6.0 g) (66). For mechanical hyperalgesia, the animals were placed on an elevated grid, and a pin-prick test was performed using a 27-gauge needle. The central part of the plantar surface of the hind paw was briefly stimulated with an intensity that was sufficient to indent but not penetrate the skin. Five minutes were set between two adjacent stimuli to the same animal. A positive response was defined as withdrawing, lifting, shaking, or licking the hind paw, and was measured by determining the number of responses of five stimuli. For the cold allodynia test, a drop of acetone solution was carefully applied onto the central plantar surface of the paw, using a blunt needle connected to a syringe (66). Two minutes were set between two adjacent stimuli, and the number of responses was calculated in the same way as the pin-prick test. After axotomy, the onset, extent, and proportion of autotomy were recorded by using the modified previously published methods (67, 68).

Electrophysiology. Data were obtained from 21 animals: four from heterozygous control mice, seven from control mice treated with CoQ10, five from db^-/db^- mice, and five from db^-/db^- mice treated with CoQ10. The in vivo experiments were complemented by in vitro experiments. From each mouse in vivo measurements were performed on one sciatic nerve, and both sciatic nerves were excised and used for the in vitro experiments. For in vivo experiments, the animals were anesthetized with 3% (vol/vol) isofluorane (Forene) and kept on a thermostat-adjusted heating pad to maintain normal body temperature (34 °C). The microsurgery was performed using aseptic technique and an operating stereomicroscope (ZEISS OPMI-9; Carl Zeiss). The left sciatic nerve was exposed through an incision, splitting the gluteal muscle and the femoral biceps. The sciatic nerve and its tibial branch to the lateral gastrocnemius muscle were exposed bilaterally. Motor CV was assessed by stimulating the sciatic nerve with single electrical pulses of 0.1-ms duration and supramaximal intensity, delivered by a pair of platinum-tipped hook electrodes. The electrodes were placed at the sciatic nerve and at the tibial branch at a distance of 6–10 mm from each other.

Recording and reference needle electrodes were placed in the lateral head of the gastrocnemius muscle. A ground wire was placed in the adductor group of muscles. The evoked compound action potential was recorded and displayed on an oscilloscope (Medelec Synergy MS-91; Oxford Instruments). Responses were recorded with a Multitec ×2222 electrometer amplifier and stored on computer with a record system. The CV was calculated for the impulses passing between the two stimulation electrodes (one at the sciatic and one at the tibial nerve) by recording the responses of the gastrocnemius muscle to the stimulation at the two sites and by dividing the distance between the stimulation sites (measured with a slide caliper) with the time difference between the resulting compound action potentials (Fig. 2*A*).

After the recording session, the section between midthigh and midcalf of the sciatic nerve and its branches, the sural, tibial, and peroneal nerves, was excised and transferred into a chamber with Ringer solution (149 mM NaCl, 5.9 mM KCl, 3.0 mM $CaCl_2$, 10.0 Hepes, adjusted to pH 7.4 with NaOH). For in vitro experiments, the two sciatic nerves from each in vivo experiment were cut in suitable lengths (11–15 mm) and transferred to a temperature-regulated Perspex chamber containing Ringer solution and two fixed Ag/AgCl recording electrodes. Two movable Ag/AgCl stimulating electrodes, along with a ground electrode, were immersed onto the proximal end of the nerve and 10-μs voltage pulses of about twice threshold amplitude were delivered. The distance between the stimulating electrode and the first recording electrode was measured with a caliper. Action currents were amplified 1,000-fold and sampled at 100 kHz using Clampex 8.2 together with a Digidata 1200A acquisition board (Molecular Devices). Most measurements were made at room temperature, but we also performed experiments at varying temperatures (5–35 °C) to obtain a quantitative estimation of the temperature dependence. The time from stimulation artifact to the compound action potential peak was used as a measure for the calculation of the nerve CV to get robust data, uncontaminated by the stimulation artifact (Fig. 2*B*). Data were analyzed, using Mathematica 7.0 (Wolfram Research) and custom written software.

Western Blot Analysis. Total protein of lumbar (L) 4 and L5 DRGs from db^-/db^- and control mice (32/33 WoA) was extracted and processed for Western blot. Briefly, DRGs were homogenized in RIPA lysis buffer (50 mM Tris•HCl, pH 7.4, 1% Nonidet P-40, 0.25% sodium deoxycholate, 150 mM NaCl, 1 mM EDTA, 1 mM NaF, and 1 mM Na3VO4) containing protease inhibitor mixture (Sigma). After sonication, lysates was centrifuged at 15,000 × *g* for 20 min at 4 °C. The supernatant was collected and protein concentration was measured by Bradford's Assay (Bio-Rad). Next, 1× laemmli sample buffer containing 20 μg protein was loaded in each lane and separated on 10% (wt/vol) SDS/PAGE gel, then transferred to polyvinylidene fluoride (PVDF) membranes (Millipore). Membranes were blocked with 5% (wt/vol) nonfat dry milk in TBS with 0.1% Tween-20 for 1 h at room temperature and incubated overnight at 4 °C with primary antibodies, including β-Actin (Mouse, 1:10,000), Bax (Rabbit, 1:5,000), Bcl-2 (Rabbit, 1:5,000), Erk1/2 (Rabbit, 1:5,000), GAPDH (Rabbit, 1:10,000), p-Akt (Rabbit, 1:1,000), p-Erk1/2 (Rabbit, 1:5,000) (all from Cell Signaling Technology), and primary guinea pig antibody of PLCβ3 (69) (1:5,000) in TBST buffer with 5% (wt/vol) BSA. After the 3× wash in TBST (10 min for each time), the membranes were incubated with HRP-con-

jugated secondary antibodies in TBST buffer containing 5% nonfat dry milk for 1 h at room temperature (1: 5,000–1: 10,000; Dako). The membranes were incubated with ECL solution for 5 min (Amersham Biosciences) after the wash step and exposed to X-ray film (NEN PerkinElmer).

Immunohistochemistry. Animals were deeply anesthetized with sodium pentobarbital (Mebumal; 50 mg/kg, i.p.), and transcardially perfused with 20 mL warm saline (0.9%; 37 °C), followed by 20 mL of a warm mixture of paraformaldehyde (4% (wt/vol); 37 °C) with 0.4% picric acid in 0.16 M phosphate buffer (pH 7.2) (70, 71), and then by 50 mL of the same, but ice-cold fixative. The L5 DRGs were dissected out and postfixed in the same fixative for 90 min at 4 °C and subsequently stored in 10% (wt/vol) sucrose in 0.1 M phosphate-buffer containing 0.01% sodium azide (PBS; pH 7.4; Sigma) and 0.02% Bacitracin (Sigma) at 4 °C for 2 d. Tissues were embedded with OCT compound (Tissue Tek; Miles Laboratories), frozen, and cut in a cryostat (Microm) at 12-μm thickness and mounted onto chrome alum-gelatin–coated slides.

The sections were dried at room temperature for 30 min, and then rinsed in PBS for 15 min and incubated for 24 h at 4 °C in a humid chamber with polyclonal rabbit antisera raised against the following markers: CGRP (1:10,000) (72), galanin (1:8,000) (73), NPY (1:4,000) (Peninsula Laboratories), substance P (SP, 1: 4,000) (Cell Signaling Technology), PLCβ3 (69), Iba1 (Vector Laboratories), SOD2 (1:5,000) (Cell Signaling Technology), GFAP (1:4,000) (Cell Signaling Technology), and p-p38 (1:400) (Cell Signaling Technology). The antisera were diluted in PBS containing 0.2% (wt/vol) BSA, 0.03% Triton X-100 (Sigma). Immunoreactivity was visualized using a commercial kit (TSA Plus, NEN Life Science Products). Briefly, the slides were rinsed in TNT buffer (0.1 M Tris•HCL, pH 7.5; 0.15 M NaCl; 0.05% Tween 20) for 15 min at room temperature, blocked with TNB buffer (0.1 M Tris•HCL; pH 7.5; 0.15 M NaCl; 0.5% Du Pont Blocking Reagent) for 30 min at room temperature followed by 30-min incubation with HRP-labeled secondary antibody (1:200) (Dako) diluted in TNB buffer. After a simple wash (15 min) in TNT buffer, all sections were exposed to biotinyl tyramide-fluorescein (1:100) diluted in amplification solution for ∼15 min, washed in TNT buffer for 30 min at room temperature, and counterstained for 15 min in 0.001% (wt/vol) propidium iodide (PI) (Sigma) in PBS. Finally, all slides were coverslipped with glycerol/PBS (9:1) containing 0.1% (wt/vol) para-phenylenediamine (74, 75). The sections were analyzed in a Bio-Rad Radiance Plus confocal scanning microscope (Bio-Rad) installed on a Nikon Eclipse E 600 fluorescence microscope equipped with 10× (0.5 N.A.), 20× (0.75 N.A.), and 60× oil (1.40 N.A.) objectives. The fluorescein labeling was excited using the 488-nm line of the argon ion laser and detected after passing a HQ 530/60 (Bio-Rad) emission filter. For the detection of PI, the 543-nm line of the green HeNe laser was used in combination with the HQ 570 (Bio-Rad) emission filter.

The specificity of antisera was examined by preincubation antisera with their homologous antigens, with the exception of the PLCβ3 antiserum. For specificity test, see Nomura et al. (69). After the preadsorption experiments, no immunoreactive neuron could be observed.

Neuron Profile Counting. To determine the percentage of immunoreactive (IR) neuron profiles (NPs), the counting was performed on 12-μm-thick sections, and every fourth or sixth section was selected (Nike Microphot-FX microscope, 20× objectives). The total number of immunopositive NPs was divided by the total number of PI-stained NPs in the DRG sections (33), and the percentage of positive NPs was calculated. Five to 10 sections of each DRG from five animals in each group were included in the analysis, and 1,200–3,000 NPs were counted in each ganglion. The size distribution of NPs with a visible nucleus was measured using the Nikon Eclipse E 600 fluorescence microscope with Wasabi Image Software. We divided the NPs into small (a somal area of 100–600 μm^2); medium-sized (600–1,400 μm^2), and large (>1,400 μm^2) according to earlier studies (33, 76). The percentages of DRG NPs in each of these categories were calculated.

Stereology. To measure the total number of L5 DRG neurons, stereological counting methods were used (77). The methods have previously been described in detail (33). Briefly, L5 DRGs from db^-/db^- and heterozygous control mice were dissected out after perfusion (as mentioned above) and randomly rotated around their axis and embedded with OCT compound, then frozen and cut in 30-μm-thick serial sections. The sections were counterstained in 0.001% PI. Every third section was systematically sampled with a random starting point. Between 7 and 17 sections were examined through the extent of each ganglion. The counting was performed using a Leica TCS SPE Systems (D-35578) confocal laser-scanning system. Images were recorded with either a 63×/ 1.3 oil-immersion objective or a 5×/0.15 air objective and stored in a computer for subsequent analysis with LAS AF SPE Core Application Software (Leica Application Suite, Leica-Microsystems.Com). The Cavalieri method (78) was used to estimate the volume of the DRG. The cross-sectional area of each ganglion was measured with the 5× objective by using SPE Core Application Software. Axial scan was used to measure the thickness of sections in a random systematic fashion across each section with the 63× objective. The total ganglion volume was calculated by multiplying the mean cross-sectional area, mean section thickness, and total number of sections of the DRG. The sampling scheme used was based on the results from a pilot study, in which the appropriate number of disector was determined. In total, a mean of 26 disector was analyzed in each ganglion. With a random starting point in each section, every fifth field was systematically sampled. At each location, optical sectioning was performed with the confocal laser-scanning system (63×/1.3 oil objective). The starting point, which was derived from a *z*-scan, was set 3- to 7-μm below the section surface. From this point, 13 consecutive optical sections were recorded by using a *z*-axis step size of 1 μm. The resulting stack of digital images was analyzed on a computer equipped with the SPE Core Application Software. An unbiased counting frame with an area of 30,976 μm^2 was presented by the computer and all neurons with a nucleolus in the starting plane or in the guard volume, which includes the immediately adjacent mechanical section, were disregarded. In the following 12 sections (i.e., sections 2–13), all neurons with a distinct nucleolus appearing inside the counting frame were counted. In this way, by using an optical disector with a height of 12 μm, an average of 105 neurons was sampled in each ganglion. The neuron density was calculated as the sum of all neurons counted divided by the summed volume of all disector. The number of neurons was calculated as the product of the DRG volume and the numerical density.

In Situ Hybridization. The db^-/db^- and heterozygous control mice used for in situ hybridization were decapitated and DRGs were rapidly dissected and frozen on dry ice. Tissues were cut in a cryostat (Microm) at 12-μm thickness, thaw-mounted on Superfrost slides (Fisher Scientific) and stored at −20 °C. From the series, the first of every four sections were subjected to in situ hybridization. The sequences of the synthetic oligonucleotides complementary to mRNA encoding PLCβ3 were 5′-TCCTTGTGTCCCTGATGGAGCTGATGTCCAGTGTGTCCACCTCCA-3′ and 5′-GTGTTCCGGGAGGCGTTCTGAGCCAATATGTTCATGGCCAGTTTA-3′ (79). Probes were synthesized by Cybergene AB and labeled at the 3′-end with [^{33}P] ATP (Perkin-Elmer) using terminal deoxynucleotidyl transferase (Amersham) to a specific

activity of 2.8–6.0 × 10^7 cpm/μg. The labeled oligoprobes were purified using ProbeQuant G-50 Micro Columns (Amersham). Sections were hybridized as described previously (80, 81). Briefly, air-dried sections were incubated in a hybridization mixture [50% (vol/vol) formamide, 4× SSC, 1× Denhardt's solution 1% sarcosyl, 0.02 M phosphate buffer, pH 7.6, 10% (wt/vol) dextran sulfate, 500 μg/mL heat-denatured salmon sperm DNA, and 1 × 10^7 cpm/mL of the labeled probe] in a humidified chamber for 18 h at 42 °C. After hybridization, the sections were washed in 1× SSC for 4 × 15 min at 55 °C and 30 min at room temperature, then air-dried and dipped into Kodak NTB 2 emulsion (Kodak) diluted 1:1 with water. After exposure at 4 °C for 2 wk, the slides were developed in Kodak D19, fixed in Kodak Unifix and mounted in glycerol-phosphate buffer. For specificity control, adjacent sections were incubated with an excess (100×) of unlabeled probe.

1. Hummel KP, Dickie MM, Coleman DL (1966) Diabetes, a new mutation in the mouse. *Science* 153(3740):1127–1128.
2. Chen H, et al. (1996) Evidence that the diabetes gene encodes the leptin receptor: Identification of a mutation in the leptin receptor gene in db/db mice. *Cell* 84(3):491–495.
3. Lee GH, et al. (1996) Abnormal splicing of the leptin receptor in diabetic mice. *Nature* 379(6566):632–635.
4. Chua SC, Jr., et al. (1996) Phenotypes of mouse diabetes and rat fatty due to mutations in the OB (leptin) receptor. *Science* 271(5251):994–996.
5. Halaas JL, et al. (1995) Weight-reducing effects of the plasma protein encoded by the obese gene. *Science* 269(5223):543–546.
6. Eliasson SG (1964) Nerve conduction changes in experimental diabetes. *J Clin Invest* 43:2353–2358.
7. Powell H, et al. (1977) Alloxan diabetic neuropathy: Electron microscopic studies. *Neurology* 27(1):60–66.
8. Sharma AK, Thomas PK (1974) Peripheral nerve structure and function in experimental diabetes. *J Neurol Sci* 23(1):1–15.
9. McMurray F, Cox RD (2011) Mouse models and type 2 diabetes: Translational opportunities. *Mamm Genome* 22(7–8):390–400.
10. Shafrir E, Sima A (2000) *Animal Models in Diabetes (e-book). A Primer* (Taylor & Francis, Abingdon, Oxford).
11. Pande M, et al. (2011) Transcriptional profiling of diabetic neuropathy in the BKS db/db mouse: A model of type 2 diabetes. *Diabetes* 60(7):1981–1989.
12. Sullivan KA, et al. (2007) Mouse models of diabetic neuropathy. *Neurobiol Dis* 28(3): 276–285.
13. Kamiya H, Murakawa Y, Zhang W, Sima AA (2005) Unmyelinated fiber sensory neuropathy differs in type 1 and type 2 diabetes. *Diabetes Metab Res Rev* 21(5):448–458.
14. Roane DS, Porter JR (1986) Nociception and opioid-induced analgesia in lean (Fa/-) and obese (fa/fa) Zucker rats. *Physiol Behav* 38(2):215–218.
15. Goto Y, Kakizaki M, Yagihashi S (1982) Neurological findings in spontaneously diabetic rats. *Excerpta Medica ICS* 581:26–38.
16. Drel VR, et al. (2006) The leptin-deficient (ob/ob) mouse: A new animal model of peripheral neuropathy of type 2 diabetes and obesity. *Diabetes* 55(12):3335–3343.
17. Bevington PR (1969) *Data Reduction and Error Analysis for the Physical Sciences* (McGraw-Hill, New York).
18. Chapman RA (1967) Dependence on temperature of the conduction velocity of the action potential of the squid giant axon. *Nature* 213(5081):1143–1144.
19. Frankenhaeuser B, Moore LE (1963) The effect of temperature on the sodium and potassium permeability changes in myelinated nerve fibres of *Xenopus laevis*. *J Physiol* 169:431–437.
20. Hodgkin AL, Katz B (1949) The effect of temperature on the electrical activity of the giant axon of the squid. *J Physiol* 109(1–2):240–249.
21. Leinninger GM, et al. (2006) Mitochondria in DRG neurons undergo hyperglycemic mediated injury through Bim, Bax and the fission protein Drp1. *Neurobiol Dis* 23(1):11–22.
22. Russell JW, et al. (2002) High glucose-induced oxidative stress and mitochondrial dysfunction in neurons. *FASEB J* 16(13):1738–1748.
23. Russell JW, Sullivan KA, Windebank AJ, Herrmann DN, Feldman EL (1999) Neurons undergo apoptosis in animal and cell culture models of diabetes. *Neurobiol Dis* 6(5): 347–363.
24. Leinninger GM, Backus C, Uhler MD, Lentz SI, Feldman EL (2004) Phosphatidylinositol 3-kinase and Akt effectors mediate insulin-like growth factor-I neuroprotection in dorsal root ganglia neurons. *FASEB J* 18(13):1544–1546.
25. Schmeichel AM, Schmelzer JD, Low PA (2003) Oxidative injury and apoptosis of dorsal root ganglion neurons in chronic experimental diabetic neuropathy. *Diabetes* 52(1):165–171.
26. Cheng C, Zochodne DW (2003) Sensory neurons with activated caspase-3 survive long-term experimental diabetes. *Diabetes* 52(9):2363–2371.
27. Walsh GS, Orike N, Kaplan DR, Miller FD (2004) The invulnerability of adult neurons: A critical role for p73. *J Neurosci* 24(43):9638–9647.
28. Wright DE, Ryals JM, McCarson KE, Christianson JA (2004) Diabetes-induced expression of activating transcription factor 3 in mouse primary sensory neurons. *J Peripher Nerv Syst* 9(4):242–254.
29. Tsujino H, et al. (2000) Activating transcription factor 3 (ATF3) induction by axotomy in sensory and motoneurons: A novel neuronal marker of nerve injury. *Mol Cell Neurosci* 15(2):170–182.
30. Tatemoto K, Rökaeus A, Jörnvall H, McDonald TJ, Mutt V (1983) Galanin—A novel biologically active peptide from porcine intestine. *FEBS Lett* 164(1):124–128.
31. Branchek TA, Smith KE, Gerald C, Walker MW (2000) Galanin receptor subtypes. *Trends Pharmacol Sci* 21(3):109–117.
32. Shi TJ, et al. (2006) Sensory neuronal phenotype in galanin receptor 2 knockout mice: Focus on dorsal root ganglion neurone development and pain behaviour. *Eur J Neurosci* 23(3):627–636.
33. Shi TJ, et al. (2001) Effect of peripheral nerve injury on dorsal root ganglion neurons in the C57 BL/6J mouse: Marked changes both in cell numbers and neuropeptide expression. *Neuroscience* 105(1):249–263.
34. Zochodne DW, Verge VM, Cheng C, Sun H, Johnston J (2001) Does diabetes target ganglion neurones? Progressive sensory neurone involvement in long-term experimental diabetes. *Brain* 124(Pt 11):2319–2334.
35. Dumoulin FL, Raivich G, Streit WJ, Kreutzberg GW (1991) Differential regulation of calcitonin gene-related peptide (CGRP) in regenerating rat facial nucleus and dorsal root ganglion. *Eur J Neurosci* 3(4):338–342.
36. Noguchi K, Senba E, Morita Y, Sato M, Tohyama M (1990) Alpha-CGRP and beta-CGRP mRNAs are differentially regulated in the rat spinal cord and dorsal root ganglion. *Brain Res Mol Brain Res* 7(4):299–304.
37. Jessell T, Tsunoo A, Kanazawa I, Otsuka M (1979) Substance P: Depletion in the dorsal horn of rat spinal cord after section of the peripheral processes of primary sensory neurons. *Brain Res* 168(2):247–259.
38. Nielsch U, Keen P (1989) Reciprocal regulation of tachykinin- and vasoactive intestinal peptide-gene expression in rat sensory neurones following cut and crush injury. *Brain Res* 481(1):25–30.
39. Nielsch U, Bisby MA, Keen P (1987) Effect of cutting or crushing the rat sciatic nerve on synthesis of substance P by isolated L5 dorsal root ganglia. *Neuropeptides* 10(2):137–145.
40. Hökfelt T, Zhang X, Wiesenfeld-Hallin Z (1994) Messenger plasticity in primary sensory neurons following axotomy and its functional implications. *Trends Neurosci* 17(1):22–30.
41. Costigan M, et al. (2002) Replicate high-density rat genome oligonucleotide microarrays reveal hundreds of regulated genes in the dorsal root ganglion after peripheral nerve injury. *BMC Neurosci* 3:16.
42. Xiao HS, et al. (2002) Identification of gene expression profile of dorsal root ganglion in the rat peripheral axotomy model of neuropathic pain. *Proc Natl Acad Sci USA* 99(12):8360–8365.
43. Burnand RC, Price SA, McElhaney M, Barker D, Tomlinson DR (2004) Expression of axotomy-inducible and apoptosis-related genes in sensory nerves of rats with experimental diabetes. *Brain Res Mol Brain Res* 132(2):235–240.
44. Brussee V, et al. (2008) Distal degenerative sensory neuropathy in a long-term type 2 diabetes rat model. *Diabetes* 57(6):1664–1673.
45. Cheng HT, et al. (2010) p38 mediates mechanical allodynia in a mouse model of type 2 diabetes. *Mol Pain* 6:28.
46. Hökfelt T, et al. (2012) *Neuropeptides in Neuroprotection and Neuroregeneration*, ed Nyberg F (Taylor & Frances, Abingdon), pp 1–15.
47. Kerekes N, Mennicken F, O'Donnell D, Hökfelt T, Hill RH (2003) Galanin increases membrane excitability and enhances Ca(2+) currents in adult, acutely dissociated dorsal root ganglion neurons. *Eur J Neurosci* 18(11):2957–2966.
48. Sten Shi TJ, Zhang X, Holmberg K, Xu Z-QD, Hökfelt T (1997) Expression and regulation of galanin-R2 receptors in rat primary sensory neurons: Effect of axotomy and inflammation. *Neurosci Lett* 237(2–3):57–60.
49. Xu Z-Q, Shi T-J, Hökfelt T (1996) Expression of galanin and a galanin receptor in several sensory systems and bone anlage of rat embryos. *Proc Natl Acad Sci USA* 93(25):14901–14905.
50. Zhang X, et al. (1993) Marked increase in cholecystokinin B receptor messenger RNA levels in rat dorsal root ganglia after peripheral axotomy. *Neuroscience* 57(2): 227–233.
51. Quinzii CM, Hirano M (2010) Coenzyme Q and mitochondrial disease. *Dev Disabil Res Rev* 16(2):183–188.
52. Negi G, Kumar A, Joshi RP, Sharma SS (2011) Oxidative stress and Nrf2 in the pathophysiology of diabetic neuropathy: Old perspective with a new angle. *Biochem Biophys Res Commun* 408(1):1–5.
53. Pop-Busui R, Sima A, Stevens M (2006) Diabetic neuropathy and oxidative stress. *Diabetes Metab Res Rev* 22(4):257–273.
54. Honma H, Podratz JL, Windebank AJ (2003) Acute glucose deprivation leads to apoptosis in a cell model of acute diabetic neuropathy. *J Peripher Nerv Syst* 8(2): 65–74.
55. Kellogg AP, Pop-Busui R (2005) Peripheral nerve dysfunction in experimental diabetes is mediated by cyclooxygenase-2 and oxidative stress. *Antioxid Redox Signal* 7(11-12): 1521–1529.
56. Vincent AM, et al. (2007) SOD2 protects neurons from injury in cell culture and animal models of diabetic neuropathy. *Exp Neurol* 208(2):216–227.
57. Negi G, Kumar A, Sharma SS (2011) Melatonin modulates neuroinflammation and oxidative stress in experimental diabetic neuropathy: Effects on NF-κB and Nrf2 cascades. *J Pineal Res* 50(2):124–131.
58. Cameron NE, Cotter MA, Archibald V, Dines KC, Maxfield EK (1994) Anti-oxidant and pro-oxidant effects on nerve conduction velocity, endoneurial blood flow and oxygen tension in non-diabetic and streptozotocin-diabetic rats. *Diabetologia* 37(5):449–459.
59. Chen AS, et al. (2004) Pyridoxal-aminoguanidine adduct is more effective than aminoguanidine in preventing neuropathy and cataract in diabetic rats. *Horm Metab Res* 36(3):183–187.
60. Gruber J, Schaffer S, Halliwell B (2008) The mitochondrial free radical theory of ageing—Where do we stand? *Front Biosci* 13:6554–6579.
61. Florence TM (1995) The role of free radicals in disease. *Aust N Z J Ophthalmol* 23(1):3–7.

62. Giugliano D (2000) Dietary antioxidants for cardiovascular prevention. *Nutr Metab Cardiovasc Dis* 10(1):38–44.
63. Lenaz G, et al. (2000) Mitochondrial bioenergetics in aging. *Biochim Biophys Acta* 1459(2-3):397–404.
64. Linnane AW, Kios M, Vitetta L (2007) The essential requirement for superoxide radical and nitric oxide formation for normal physiological function and healthy aging. *Mitochondrion* 7(1–2):1–5.
65. McCarty MF (2010) Practical prevention of cardiac remodeling and atrial fibrillation with full-spectrum antioxidant therapy and ancillary strategies. *Med Hypotheses* 75 (2):141–147.
66. Shi TJ, et al. (2008) Phospholipase Cbeta3 in mouse and human dorsal root ganglia and spinal cord is a possible target for treatment of neuropathic pain. *Proc Natl Acad Sci USA* 105(50):20004–20008.
67. Kotulska K, et al. (2006) Overexpression of copper/zinc-superoxide dismutase in transgenic mice markedly impairs regeneration and increases development of neuropathic pain after sciatic nerve injury. *J Neurosci Res* 84(5):1091–1097.
68. Koplovitch P, Minert A, Devor M (2012) Spontaneous pain in partial nerve injury models of neuropathy and the role of nociceptive sensory cover. *Exp Neurol* 236(1): 103–111.
69. Nomura S, Fukaya M, Tsujioka T, Wu D, Watanabe M (2007) Phospholipase Cbeta3 is distributed in both somatodendritic and axonal compartments and localized around perisynapse and smooth endoplasmic reticulum in mouse Purkinje cell subsets. *Eur J Neurosci* 25(3):659–672.
70. Pease PC (1962) Buffered formaldehyde as a killing agent and primary fixative for electron microscopy. *Anat Rec* 142:342.
71. Zamboni I, De Martino C (1967) Buffered picric acid formaldehyde. A new rapid fixative for electron microscopy. *J Cell Biol* 35:148A.
72. Orazzo C, Pieribone VA, Ceccatelli S, Terenius L, Hökfelt T (1993) CGRP-like immunoreactivity in A11 dopamine neurons projecting to the spinal cord and a note on CGRP-CCK cross-reactivity. *Brain Res* 600(1):39–48.
73. Theodorsson E, Rugarn O (2000) Radioimmunoassay for rat galanin: Immunochemical and chromatographic characterization of immunoreactivity in tissue extracts. *Scand J Clin Lab Invest* 60(5):411–418.
74. Johnson GD, Nogueira Araujo GM (1981) A simple method of reducing the fading of immunofluorescence during microscopy. *J Immunol Methods* 43(3):349–350.
75. Platt JL, Michael AF (1983) Retardation of fading and enhancement of intensity of immunofluorescence by *p*-phenylenediamine. *J Histochem Cytochem* 31(6):840–842.
76. Dubovy P, Svizenska I, Vega JA (1990) Non-specific cholinesterase activity in mouse spinal ganglia. The usefulness of histochemical study and image analysis for simple characterization of neuron subclasses. *Cell Mol Biol* 36(1):23–40.
77. Tandrup T (1993) A method for unbiased and efficient estimation of number and mean volume of specified neuron subtypes in rat dorsal root ganglion. *J Comp Neurol* 329(2):269–276.
78. Gundersen HJ, Jensen EB (1987) The efficiency of systematic sampling in stereology and its prediction. *J Microsc* 147(Pt 3):229–263.
79. Watanabe M, et al. (1998) Patterns of expression for the mRNA corresponding to the four isoforms of phospholipase Cbeta in mouse brain. *Eur J Neurosci* 10(6):2016–2025.
80. Schalling M, et al. (1988) Neuropeptide tyrosine in the rat adrenal gland—Immunohistochemical and in situ hybridization studies. *Neuroscience* 24(1):337–349.
81. Dagerlind Å, Friberg K, Bean AJ, Hökfelt T (1992) Sensitive mRNA detection using unfixed tissue: combined radioactive and non-radioactive in situ hybridization histochemistry. *Histochemistry* 98(1):39–49.

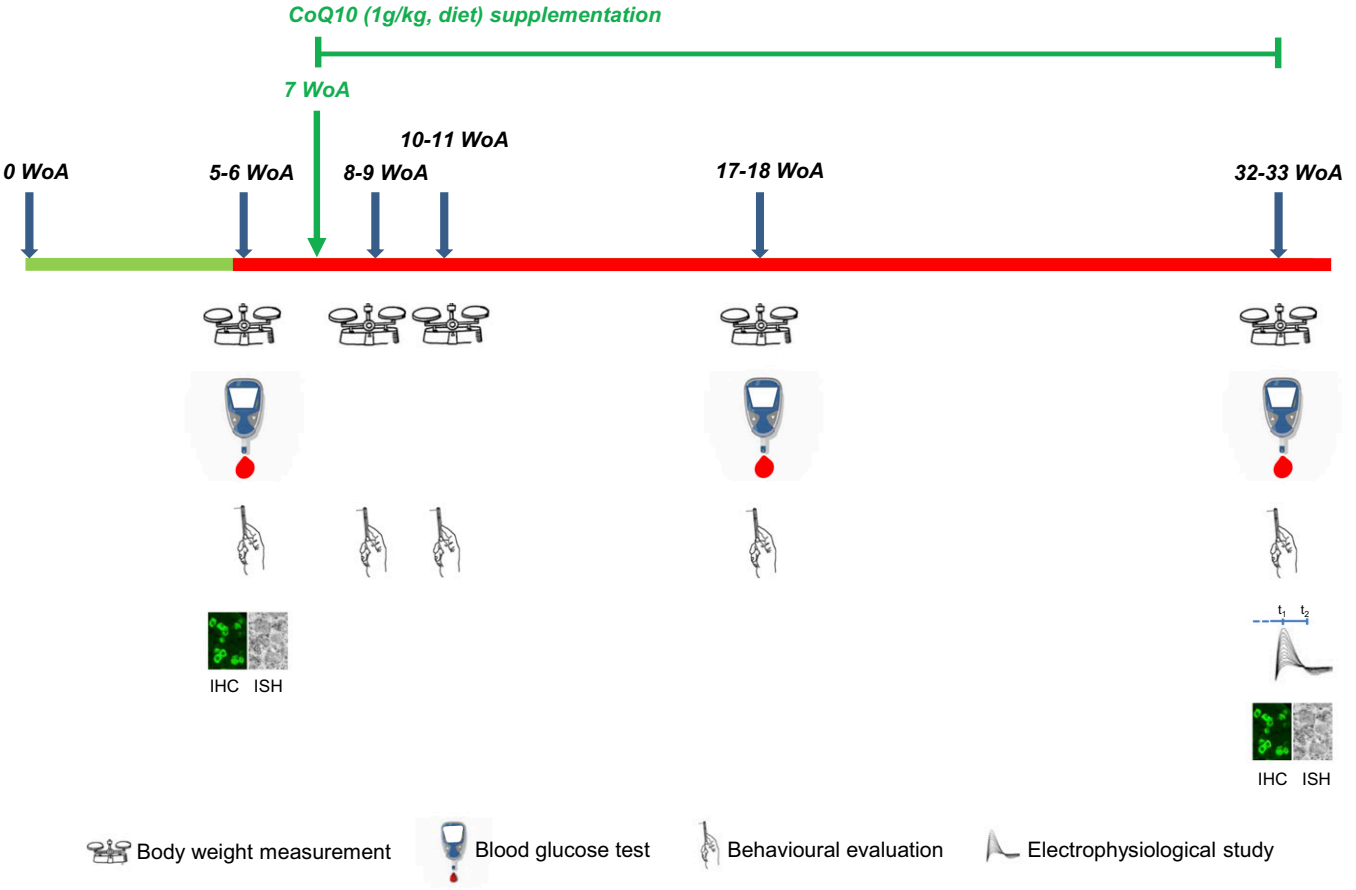

Fig. S1. Schematic overview of the experimental procedures. Behavioral evaluation performed using the von Frey filaments, acetone, and pin-prick tests. Animals killed at 5–6 or 32–33 WoA for immunohistochemistry (IHC), in situ hybridization (ISH), or electrophysiology (E-PHYS).

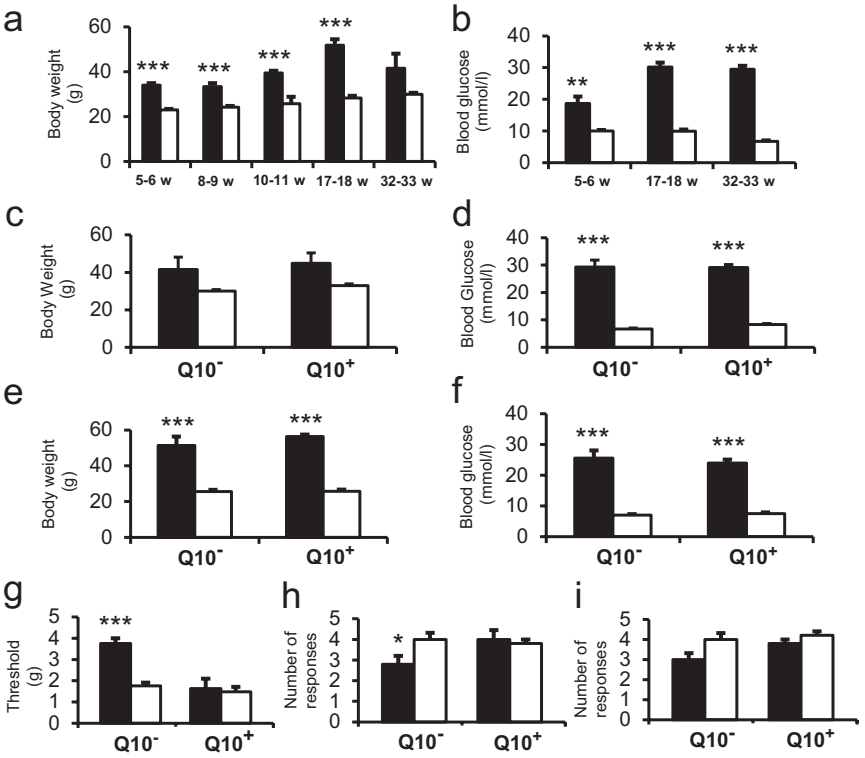

Fig. S2. (*A* and *B*) Body weight (*A*) and blood-glucose levels (*B*) in male diabetic mice at different weeks of age. (*C–F*) CoQ10 treatment has no effect on body weight or blood-glucose levels in male (*C* and *D*) or female (*E* and *F*) diabetic mice at 32/33 WoA, respectively. (*G–I*) Response to innoxious (*G*), noxious (*I*), or cold (*H*) stimulations in db^{-}/db^{-} and control female mice with or without CoQ10 treatment, at 32/33 WoA . Q10-, Q10-untreated; Q10+, Q10-treated. Filled columns, db^{-}/db^{-}; open columns, control. The data are shown as mean ± SEM, $^{*}P < 0.05$, $^{**}P < 0.01$, $^{***}P < 0.001$ vs. control; n = 5–20 mice.

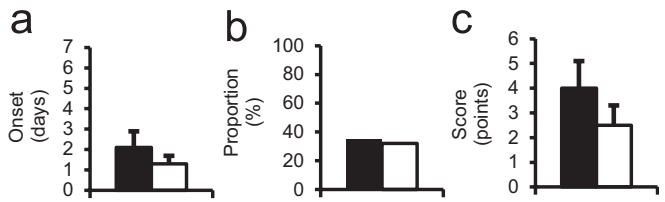

Fig. S3. (*A–C*) Autotomy after unilateral axotomy in male mice at 32–33 WoA. (*A*) The average onset of autotomy was slightly delayed in db^{-}/db^{-} mice but not statistically significant compared with control mice ($P > 0.05$). (*B*) At day 7 after axotomy, autotomy in the ipsilateral hind paw was seen in around 35% of animals in both diabetic and control groups. (*C*) The average autotomy score in diabetic group was similar as in control group ($P > 0.05$). Filled columns, db^{-}/db^{-}; open columns, control. The data are shown as mean ± SEM, n = 6–18 mice.

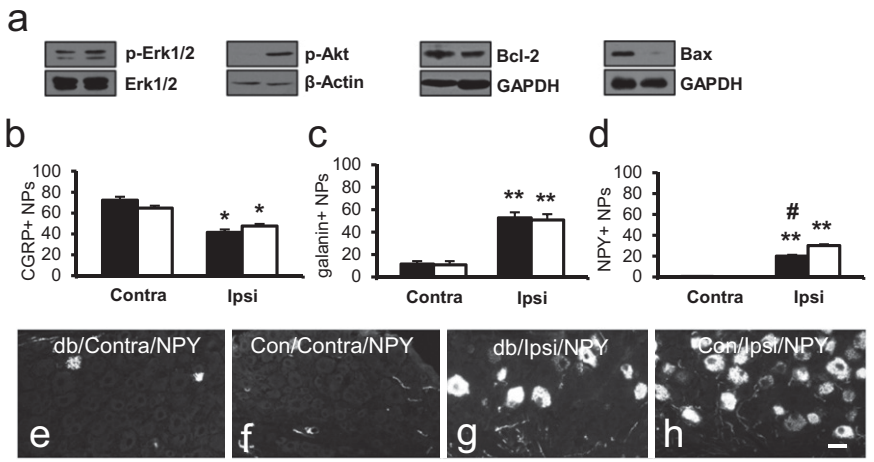

Fig. S4. (*A*) Prosurvival and apoptotic related proteins examined by Western blot in DRGs of 32/33 WoA male db^{-}/db^{-} (*Left* bands) and control (*Right* bands) mice. (*B–H*) Effect of unilateral axotomy (7 d) on neuropeptide expression in DRGs in male db^{-}/db^{-} mice. (*B–D*) Percentage of CGRP- (*B*), galanin- (*C*), and NPY- (*D*) IR NPs in contra- and ipsilateral DRGs. CGRP is decreased (*B*), and galanin (*C*) and NPY (*D*) are increased in ipsilateral DRGs in both db^{-}/db^{-} and control mice. However, the increase is smaller for NPY in db^{-}/db^{-} mice than in controls. (*E–H*) Immunofluorescence micrographs showing only few fluorescent neurons in contralateral DRGs (*E* and *F*). A strong up-regulation of NPY is seen in ipsilateral DRGs in both db^{-}/db^{-} (*G*) and control (*H*) mice but less in the former (*G* and *H*). $^{*}P < 0.05$ and $^{**}P < 0.01$ vs. contralateral DRGs in both db^{-}/db^{-} and control mice, respectively; $^{\#}P < 0.05$ vs. ipsilateral DRGs in control mice. Filled columns, db^{-}/db^{-} mice; open columns, control mice; Contra, contralateral; Ipsi, ipsilateral. The data are shown as mean ± SEM $n = 5–10$ mice. (Scale bar, *E–H*: 50 μm.)

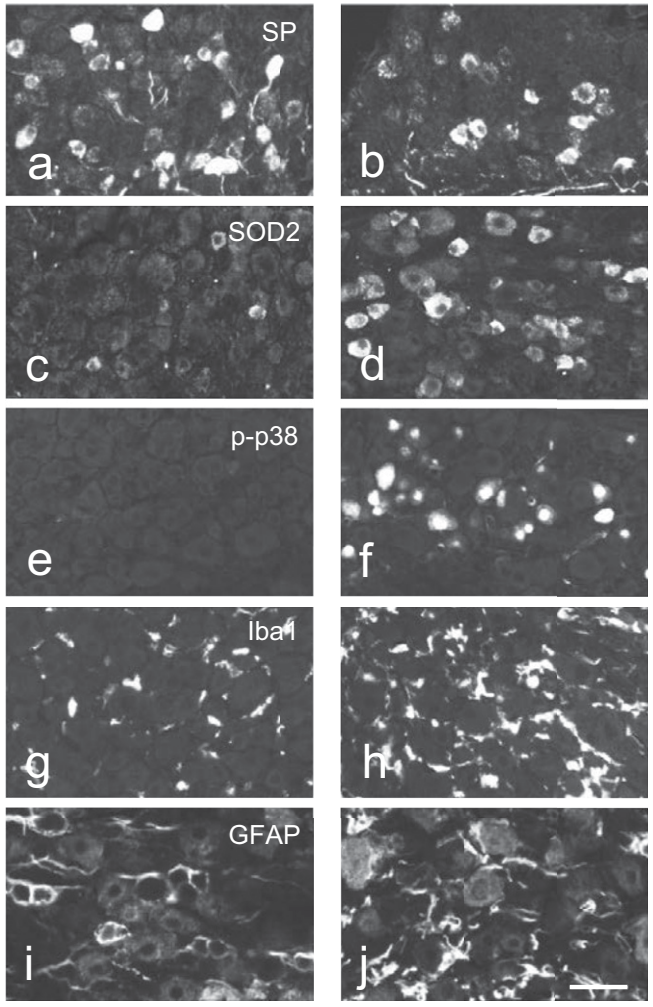

Fig. S5. Immunofluorescence micrographs showing effect of unilateral axotomy (7 d) on expression of several markers in DRGs of male db^{-}/db^{-} mice at 32–33 WoA. Substance P (SP)-LI is markedly down-regulated in ipsilateral DRG (*B*) compared with contralateral side (*A*). In contrast, SOD2, p-p38, Iba1, and GFAP-LIs are strongly up-regulated in the ipsilateral DRGs (compare *D*, *F*, *H*, *J* with *C*, *E*, *G*, *I*, respectively). (Scale bar, *A–J*: 50 μm.)

Table S1. CoQ10 prevents the decrease in impulse conduction

	In vivo		In vitro	
	Mean velocity (m/s)	C_v (%)	Mean velocity (m/s)	C_v (%)
Control	53.2 ± 3.1 (n = 4)	11.8	12.2 ± 0.7 (n = 7)	15.7
Control + Q10	49.9 ± 2.0 (n = 7)	11.4	11.3 ± 0.5 (n = 6)	11.7
Db$^-$/*db*$^-$ mice	39.2 ± 5.7 (n = 5)	32.6	8.2 ± 1.0 (n = 3)	21.0
Db$^-$/*db*$^-$ mice + Q10	52.7 ± 2.7 (n = 5)	11.4	10.3 ± 0.7 (n = 7)	18.7

C_v, coefficient of variation.

Table S2. In vivo and in vitro studies: Variance analysis (two-way ANOVA) (1) of the CV measurements

Sources of variation	Degrees of freedom	Sums of squares	Mean squares	*F* statistic	*P* value
In vivo					
Strain	1	140.90	140.90	2.1580	0.1601
Treatment	1	124.82	124.82	1.9118	0.1847
Strain + treatment	1	353.50	353.50	5.4142	0.0326
Error	17	1108.0	65.291		
Total	20	1729.2			
In vitro					
Strain	1	24.558	24.558	7.9013	0.0112
Treatment	1	0.5096	0.5096	0.1639	0.6901
Strain + treatment	1	11.819	11.819	3.8027	0.0661
Error	19	59.054	3.108		
Total	22	95.941			

1. Fisher RA (1925) Theory of statistical estimation. *Mathematical Proceedings of the Cambridge Philosophical Society* 22:700–725.

Table S3. Stereological study effects of CoQ10 treatment

	Number of DRG neurons		
	5/6 WoA (n = 6)	32/33 WoA (n = 5)	32/33 WoA/Q10 (n = 5)
Control	11,315 (SD: 2,266; C_v: 0.20)	9,643 (SD: 1,377; C_v: 0.14)	11,180 (SD:2,582; C_v: 0.24)
Db$^-$/*db*$^-$	11,447 (SD: 2,400; C_v: 0.20)	6,495 (SD: 1,868; C_v: 0.29)*	9,628 (SD: 2,567; C_v: 0.27)
Neuron loss	1.2%	32.6%	13.9%

Table S4. Primary antisera/antibodies used for immunohistochemistry and Western blot in this study

Antigen	Host	Immunogen	Source, type	Dilution
GFAP	Rabbit	GFAP from human brain	Sigma-Aldrich; G9269, Polyclonal	1:4,000
Iba1	Rabbit	A synthetic peptide corresponding to C terminus of Iba1	Wako; #01–974, Polyclonal	1:4,000
NF200	Mouse	Purified rat midsize neurofilament (NF-M) subunit	Sigma-Aldrich; N2912, Monoclonal	1:2,000
NPY	Rabbit	Synthetic NPY coupled to BSA	J. Walsh and H. Wong, Gastroenteric Biology Center, Department of Medicine, University of California Los Angeles, CA, Polyclonal	1:4,000
P2X3	Rabbit	Carboxy-terminus of rat P2X3 (amino acids 383–397)	R. Elde, Department of Cell Biology and Neuroanatomy, University of Minnesota, MN, Polyclonal	1:4,000
PLCβ3	Guinea pig	1201–1234 amino acids of mouse PLCβ3	M. Watanabe, Hokkaido University School of Medicine, Sapporo, Japan, Polyclonal	1:2,000
p-p38	Rabbit	A synthetic phosphopeptide corresponding to residues surrounding Thr180/Tyr182 of human p38 MAPK	Cell Signaling Technology; #9211, Polyclonal	1:400
SOD2	Rabbit	Full length of rat SOD2	Abcam; #ab13534, Polyclonal	1:2,000
SP	Rabbit	Synthetic SP coupled to BSA	L. Terenius, Center for Molecular Medicine, Karolinska Institutet, Stockholm, Sweden, Polyclonal	1:4,000
NPY R1	Rabbit	C-terminal portion of rat NPY Y1R (aa 370–382)	J. Walsh and H. Wong, Gastroenteric Biology Center, Department of Medicine, University of California Los Angeles, CA, Polyclonal	1:2,000
β-Actin	Mouse	A synthetic peptide corresponding to amino-terminal residues of human β-actin	Cell Signaling Technology; #3700, Monoclonal	1:5,000
Bax	Rabbit	A synthetic peptide corresponding to the amino-terminal residues of human Bax	Cell Signaling Technology; #2772, Polyclonal	1:1,000
Erk1/2	Rabbit	A synthetic peptide corresponding to a sequence in the C terminus of rat p44 MAP Kinase	Cell Signaling Technology; #9102, Polyclonal	1:1,000
GAPDH	Rabbit	A synthetic peptide near the carboxyl terminus of human GAPDH	Cell Signaling Technology; #2118, Monoclonal	1:5,000
pAkt	Rabbit	A synthetic phosphopeptide corresponding to residues surrounding Ser473 of mouse Akt	Cell Signaling Technology; #9271, Polyclonal	1:1,000
pErk1/2	Rabbit	A synthetic phosphopeptide corresponding to residues surrounding Thr202/Tyr204 of human p44 MAP kinase	Cell Signaling Technology; #9101, Polyclonal	1:2,000